

Spectroscopic amplitudes in microscopic three-cluster systems

P. Descouvemont **Physique Nucléaire Théorique et Physique Mathématique, C.P. 229, Université Libre de Bruxelles (ULB), B-1050 Brussels, Belgium*

(Received 18 November 2022; accepted 13 January 2023; published 20 January 2023)

I investigate three-body spectroscopic amplitudes in a microscopic three-cluster model. The total wave functions are described in the resonating group method (RGM) formalism based on cluster wave functions and on relative functions defined in the hyperspherical method. Core excitations are included. I develop a method aimed to determine three-body spectroscopic amplitudes and spectroscopic factors. This technique also provides three-body wave functions where the antisymmetrization is treated approximately. In this way, the various channels are orthogonal to each other and can be used without the antisymmetrization operator. This method is well known in two-cluster systems, and is based on the eigenvalues and the eigenvectors of the antisymmetrization operator. I illustrate the formalism with the ${}^6\text{He}$, ${}^{11}\text{Li}$, and ${}^{14}\text{Be}$ nuclei where ${}^9\text{Li}$ and ${}^{12}\text{Be}$ excited states are taken into account.

DOI: [10.1103/PhysRevC.107.014312](https://doi.org/10.1103/PhysRevC.107.014312)

I. INTRODUCTION

The description of exotic nuclei [1] is a challenge for theoretical models [2]. These nuclei present a low breakup threshold and the corresponding wave functions must be described accurately up to large distances. Reproducing their halo structure is crucial to investigate properties such as the radius or the quadrupole moment [3].

Microscopic models are known for a long time to provide a reliable information on the nuclear structure [4–7]. Recent *ab initio* techniques [8] are well adapted to light nuclei, but are difficult to apply to medium-mass nuclei, such as ${}^{11}\text{Li}$ or ${}^{14}\text{Be}$, which are typical examples of three-body halo structures (${}^9\text{Li} + n + n$ and ${}^{12}\text{Be} + n + n$, respectively). On the other hand, cluster models, which have been developed in the past for α nuclei [9], can be directly applied to halo nuclei. These models are based on the assumption of a cluster structure of the nucleus. A typical example is ${}^7\text{Li}$, which is seen as an $\alpha + t$ cluster structure [10]. These models have been extended to halo nuclei, where the surrounding nucleons are treated as clusters. This microscopic approach has been successfully applied to three-body nuclei such as ${}^6\text{He}$ or ${}^{11}\text{Li}$ [11–14].

In a microscopic theory, the wave function depends on all nucleon coordinates, and the information is obtained from a nucleon-nucleon interaction. The cluster approximation permits a simplification of the calculations. A halo nucleus is considered as a core surrounded by valence nucleons. Schematically, a microscopic three-body wave function involving a core and two neutrons is written as

$$\Psi = \mathcal{A}\Phi_c \Phi_n \Phi_n g, \quad (1)$$

where Φ_c is the core wave function, Φ_n is a neutron spinor, and g is the unknown relative function, to be determined

from the Schrödinger equation [4]. In this equation, \mathcal{A} is the A -nucleon antisymmetrization operator. The simplest example is the ${}^6\text{He}$ nucleus which can be described by an $\alpha + n + n$ structure [13], with a $(0s)^4$ shell-model wave function for the α particle. The relative function g is determined in the hyperspherical formalism [15], which is well adapted to three-body systems.

Recently, this theory was extended to heavier nuclei, such as ${}^{11}\text{Li}$, ${}^{14}\text{Be}$, and ${}^{17}\text{Ne}$ [14]. In these cases, the core nucleus is described in the p shell and core excitations cannot be neglected. Such calculations are very demanding in terms of numerical capabilities (computer time and memory) but are feasible with the current facilities. A limitation, however, is that the microscopic wave function (1) is difficult to interpret owing to the A -nucleon antisymmetrization. For this reason, different channels are not orthogonal to each other, and probabilities cannot be defined. In addition the relative function without antisymmetrization is not physical and cannot be used as input for other calculations.

These issues have been addressed in microscopic two-cluster models [5,16–19]. From the eigenvalues and eigenfunction of the antisymmetrization operator \mathcal{A} , the relative function g can be transformed in order to provide the so-called overlap function, and to approximate the total wave function (1) by nonantisymmetrized cluster functions [19]. The goal of the present work is to extend this formalism to three-cluster systems. This generalization provides three-body spectroscopic factors, as well as approximate radial functions, which can be used in further models, such as in distorted-wave Born approximation (DWBA) calculations [20,21].

The paper is organized as follows. In Sec. II, I present the general formalism, with a brief overview of the generator coordinate method (GCM) and of the resonating group method (RGM). I discuss in more detail the transformation of the relative function in three-body systems. Applications to ${}^6\text{He}$, ${}^{11}\text{Li}$, and ${}^{14}\text{Be}$ are presented in Sec. III. I present the conclusion and outlook in Sec. IV.

*pierre.descouvemont@ulb.be

II. THEORETICAL MODEL

A. GCM formulation

In this section, I briefly present GCM basis functions, and refer the reader to Refs. [13,14] for more detail. I consider three clusters with nucleon numbers (A_1, A_2, A_3) and internal wave functions $(\Phi_c^{S_1\nu_1}, \Phi^{S_2\nu_2}, \Phi^{S_3\nu_3})$, defined in the shell model with a common oscillator parameter b . In practice, clusters 2 and 3 are s -shell nuclei, and therefore described by a single Slater determinant (I omit the deuteron which cannot be considered as a cluster). Cluster 1, associated with the core, is a p -shell nucleus, and is described by a combination of Slater determinants. Several states (or, in other words, several S_1 values), with different spins are labeled by index c (see Ref. [22]).

The present model can be applied when the core nucleus is well described in the shell model (the theory is identical for the sd shell, but the examples considered here are in the p shell). In some cases, however, the core nucleus presents an extended density, and must be described by a multicluster approach. A typical example is ${}^8\text{He}$, which can be seen as an ${}^6\text{He}$ core, surrounded by two neutrons. As ${}^6\text{He}$ presents a halo structure, an $\alpha + n + n + n + n$ five-body model [23,24] is more suitable.

I define a channel function with total spin S by

$$\begin{aligned} \Phi_\alpha^{SM_S}(R_x, R_y) = & \mathcal{A} \left[\Phi_c^{S_1} \left(-\frac{A_{23}}{A} R_y \right) \right. \\ & \otimes \left[\Phi^{S_2} \left(\frac{A_1}{A} R_y + \frac{A_1}{A_{12}} R_x \right) \right. \\ & \left. \left. \otimes \Phi^{S_3} \left(\frac{A_1}{A} R_y - \frac{A_1}{A_{12}} R_x \right) \right]^{S_{23}} \right]^{SM_S}, \quad (2) \end{aligned}$$

where index α stands for $\alpha = (c, S_1, S_2, S_3, S_{23})$, $R_x = (R_x, \Omega_x)$ is the generator coordinate between clusters 2 and 3, and $R_y = (R_y, \Omega_y)$ between cluster 1 and the center-of-mass of system 2-3. In this equation, $A_{12} = A_1 + A_2$, $A_{23} = A_2 + A_3$, and S_{23} represents the coupling of S_2 and S_3 . Definition (2) is a combination of three-cluster Slater determinants. Notice that the generator coordinates R_x and R_y are parameters, not physical coordinates. The antisymmetrization operator \mathcal{A} does not act on these parameters.

Wave functions (2) are first projected on the orbital momenta ℓ_x and ℓ_y , associated with the coordinates R_x and R_y , respectively. The projection on the total angular momentum JM provides

$$\begin{aligned} \phi_\gamma^{JM\pi}(R_x, R_y) = & \sum_{M_L M_S} \langle LM_L SM_S | JM \rangle \\ & \times \int d\Omega_x d\Omega_y \mathcal{Y}_{\ell_x \ell_y}^{LM_L^*}(\Omega_x, \Omega_y) \Phi_\alpha^{SM_S}(R_x, R_y), \quad (3) \end{aligned}$$

where index $\gamma = (\alpha, S, L, \ell_x, \ell_y)$ and where

$$\mathcal{Y}_{\ell_x \ell_y}^{LM_L}(\Omega_x, \Omega_y) = [Y_{\ell_x}(\Omega_x) \otimes Y_{\ell_y}(\Omega_y)]^{LM_L}. \quad (4)$$

The parity π is given by

$$\pi = (-1)^K \pi_1 \pi_2 \pi_3, \quad (5)$$

where π_i is the parity of cluster i .

In the hyperspherical formalism [15,25], coordinates R_x and R_y are replaced by the hyperradius R and the hyperangle α_R by

$$\begin{aligned} R &= \sqrt{\mu_{23} R_x^2 + \mu R_y^2}, \\ \tan \alpha_R &= \sqrt{\frac{\mu}{\mu_{23}}} \frac{R_y}{R_x}, \quad (6) \end{aligned}$$

with $\mu_{23} = A_2 A_3 / A_{23}$ and $\mu = A_1 A_{23} / A$. After projection on the hyperangle, a GCM basis function is given by

$$\begin{aligned} \Phi_{\gamma K}^{JM\pi}(R) &= \int d\alpha_R F_K^{\ell_x \ell_y}(\alpha_R) \\ & \times \phi_\gamma^{JM\pi}(R \cos \alpha_R, R \sin \alpha_R) \cos^2 \alpha_R \sin^2 \alpha_R, \quad (7) \end{aligned}$$

where K is the hypermoment, and $F_K^{\ell_x \ell_y}(\alpha_R)$ is a function depending on the hyperangle (see, for example, Ref. [14]). Basis functions (7) depend on the hyperradius and on several quantum numbers. When the number of core states is large, the number of basis functions (7) strongly increases (see, for example, ${}^{11}\text{Li}$ with ${}^9\text{Li}$ excited states in Ref. [14]).

The use of GCM basis functions (7) is well adapted to numerical calculations since these functions are expressed from Slater determinants. As is well known (see for example, Ref. [5] for two-cluster systems, and Ref. [13] for three-cluster systems), basis function (7) can be written as

$$\Phi_{\gamma K}^{JM\pi}(R) = \Phi_{\text{cm}} \mathcal{A} \varphi_{\gamma K}^{JM\pi}(\Omega_5) \Gamma_K(\rho, R), \quad (8)$$

where Φ_{cm} is a center-of-mass factor. The radial functions are defined by

$$\Gamma_K(\rho, R) = \left(\frac{b^2}{\rho R} \right)^2 \left(\frac{4\pi}{b^2} \right)^{3/2} \exp\left(-\frac{\rho^2 + R^2}{2b^2} \right) I_{K+2} \left(\frac{\rho R}{b^2} \right), \quad (9)$$

where $I_K(x)$ a modified Bessel function of the first kind (see also Ref. [25]). In Eq. (8), the channel function $\varphi_{\gamma K}^{JM\pi}$ is given by

$$\begin{aligned} \varphi_{\gamma K}^{JM\pi}(\Omega_5) &= F_K^{\ell_x \ell_y}(\alpha) \left[\mathcal{Y}_{\ell_x \ell_y}^L(\Omega_x, \Omega_y) \right. \\ & \left. \otimes \left[\phi_c^{S_1}(\xi_1) \otimes [\phi^{S_2}(\xi_2) \otimes \phi^{S_3}(\xi_3)]^{S_{23}} \right]^{S_1} \right]^{JM}, \quad (10) \end{aligned}$$

where the angles $\Omega_5 = (\Omega_x, \Omega_y, \alpha)$ are associated with the physical hyperspherical coordinate ρ . In this definition, ϕ^{S_i} are translation-invariant wave functions of clusters i , and depending on the set of internal coordinates ξ_i . These internal coordinates are implied in the channel function [8].

In the GCM, the total wave function of the system is defined from a superposition of basis functions (7) as

$$\Psi^{JM\pi} = \sum_{\gamma K} \sum_{n=1}^N f_{\gamma K}^{J\pi}(R_n) \Phi_{\gamma K}^{JM\pi}(R_n), \quad (11)$$

where coefficients $f_{\gamma K}^{J\pi}(R_n)$ are referred to as the generator functions, and are obtained from a diagonalization of the Hamiltonian and overlap kernels [14]. Typically $N \approx 10$ – 15 generator coordinates are used. For scattering states, the Gaussian asymptotic behavior (9) must be corrected with the R -matrix method [26]. In the present work, however, I am only concerned with bound states, and I include large R_n values, which means that the physical asymptotic behavior of the wave functions is guaranteed for core $+n + n$ systems. In charged systems, such as core $+p + p$, the asymptotic Coulomb wave functions are approximative only, and the hyperspherical expansion is known to converge slowly (see, for example, Refs. [27,28]).

Notice that the Hamiltonian and overlap kernels require seven-dimension integrals, which are computed numerically. This represents a challenge, in particular when the core states involve many Slater determinants.

B. RGM formulation

In the resonating group method [4,5], the wave function of the system is written as

$$\Psi^{JM\pi} = \frac{1}{\rho^{5/2}} \sum_{\gamma K} \mathcal{A} g_{\gamma K}^{J\pi}(\rho) \varphi_{\gamma K}^{JM\pi}(\Omega_5), \quad (12)$$

and the relative functions $g_{\gamma K}^{J\pi}(\rho)$ are obtained from a set of integrodifferential equations

$$\sum_{\gamma' K'} \int [\mathcal{H}_{\gamma K, \gamma' K'}^{J\pi}(\rho, \rho') - E^{J\pi} \mathcal{N}_{\gamma K, \gamma' K'}^{J\pi}(\rho, \rho')] \times g_{\gamma' K'}^{J\pi}(\rho') d\rho' = 0, \quad (13)$$

where the Hamiltonian and overlap kernels are defined by

$$\begin{aligned} & \left\{ \begin{array}{l} \mathcal{N}_{\gamma K, \gamma' K'}^{J\pi}(\rho, \rho') \\ \mathcal{H}_{\gamma K, \gamma' K'}^{J\pi}(\rho, \rho') \end{array} \right\} \\ & = \langle \varphi_{\gamma K}^{JM\pi} \delta(\rho - r) | \left\{ \begin{array}{l} 1 \\ H \end{array} \right\} | \mathcal{A} \varphi_{\gamma' K'}^{JM\pi} \delta(\rho' - r) \rangle. \end{aligned} \quad (14)$$

The calculation of these kernels requires heavy analytical calculations and, in practice, the RGM is not used for microscopic three-cluster studies involving p -shell nuclei. The calculation of the overlap kernel, however, is necessary to derive spectroscopic amplitudes.

The equivalence between the GCM and the RGM is obvious with Eqs. (8), (11), and (12) which give the radial functions as

$$g_{\gamma K}^{J\pi}(\rho) = \rho^{5/2} \sum_n f_{\gamma K}^{J\pi}(R_n) \Gamma_K(\rho, R_n), \quad (15)$$

where function Γ_K is defined by Eq. (9). Function (15), however, cannot be used without the antisymmetrization operator \mathcal{A} [see Eq. (12)], since it contains a spurious contribution

from the forbidden states. This problem is well known in two-cluster systems and must be addressed by an appropriate transform (see, for example, Ref. [5]). The formalism is generalized here to three-cluster systems.

C. Three-body overlap functions

The overlap functions play an important role in transfer reactions, and are well known for two-cluster systems (see, for example, Ref. [20]). Schematically, the overlap function of a two-cluster system with wave function Ψ is given by

$$I(r) = \langle \Phi_1 \Phi_2 | \Psi \rangle, \quad (16)$$

where Φ_1 and Φ_2 are the cluster wave functions and r is the relative coordinate between the centers of mass. This definition does not depend on the model. It has been used in various microscopic theories [21,29,30]. In the simple potential model, $I(r)$ is the relative function. From the overlap integral, one defines the spectroscopic factor as

$$S = \int [I(r)]^2 dr. \quad (17)$$

In a microscopic three-cluster model, the concept of overlap integrals and spectroscopic factors remains valid (see Ref. [31] for a detailed discussion). In hyperspherical coordinates, the overlap integral in a component γK reads

$$I_{\gamma K}^{J\pi}(\rho) = \langle \varphi_{\gamma K}^{JM\pi} | \Psi^{JM\pi} \rangle, \quad (18)$$

which can be derived from the overlap kernel (14) as

$$\begin{aligned} I_{\gamma K}^{J\pi}(\rho) &= \sum_{\gamma' K'} \int \mathcal{N}_{\gamma K, \gamma' K'}^{J\pi}(\rho, \rho') g_{\gamma' K'}^{J\pi}(\rho') d\rho' \\ &= \tilde{g}_{\gamma K}^{J\pi}(\rho). \end{aligned} \quad (19)$$

Functions $\tilde{g}_{\gamma K}^{J\pi}(\rho)$ are not normalized to unity, but provide the spectroscopic factors

$$S_{\gamma K}^{J\pi} = \int |\tilde{g}_{\gamma K}^{J\pi}(\rho)|^2 d\rho. \quad (20)$$

The notation $\tilde{g}_{\gamma K}^{J\pi}(\rho)$ for the overlap integral is adopted to underline the link with functions $g_{\gamma K}^{J\pi}(\rho)$ [18]. From the overlap kernel, I derive [5]

$$\hat{g}_{\gamma K}^{J\pi}(\rho) = \sum_{\gamma' K'} \int \left(\mathcal{N}_{\gamma K, \gamma' K'}^{J\pi}(\rho, \rho') \right)^{1/2} g_{\gamma' K'}^{J\pi}(\rho') d\rho' \quad (21)$$

with the normalization

$$\sum_{\gamma K} \int [\hat{g}_{\gamma K}^{J\pi}(\rho)]^2 d\rho = 1. \quad (22)$$

This property permits one to define occupancy probabilities in the various core states, in contrast with Eq. (12) where the channel components are not orthogonal to each other.

The transformed functions \tilde{g} and \hat{g} can be written, in a compact notation, as

$$\begin{aligned} \tilde{g} &= \mathcal{N}g, \\ \hat{g} &= \mathcal{N}^{1/2}g. \end{aligned} \quad (23)$$

For the sake of clarity, I omit $J\pi$. In order to carry out these transformations, I consider the eigenvalue problem of the antisymmetrization operator

$$\mathcal{A}\chi^\alpha = \mu_\alpha \chi^\alpha, \quad (24)$$

where μ_α are the eigenvalues and χ^α the eigenvectors, written as

$$\chi^\alpha = \sum_{\gamma K} \chi_{\gamma K}^\alpha(\rho) \varphi_{\gamma K}. \quad (25)$$

Again, this problem is well known in two-cluster systems. Eigenvalues with

$$\mu_\alpha = 0 \quad (26)$$

correspond to forbidden states, which are typical antisymmetrization effects. Small eigenvalues correspond to ‘‘almost’’ forbidden states [19], and the μ_α values are contained in the [0,1] interval. From the eigenvalues μ_α and eigenvector χ^α , functions (23) are written as

$$\begin{aligned} \tilde{g}(\rho) &= \sum_{\alpha} \mu_{\alpha} \langle g | \chi^{\alpha} \rangle \chi^{\alpha}(\rho), \\ \hat{g}(\rho) &= \sum_{\alpha} \mu_{\alpha}^{1/2} \langle g | \chi^{\alpha} \rangle \chi^{\alpha}(\rho). \end{aligned} \quad (27)$$

In a few two-cluster systems (essentially between closed shell nuclei) the μ_α and χ^α are known analytically. Eigenvectors corresponding to small μ_α are short ranged. Functions (27) are conveniently written as

$$\begin{aligned} \tilde{g}(\rho) &= g(\rho) - \sum_{\alpha} (1 - \mu_{\alpha}) \langle g | \chi^{\alpha} \rangle \chi^{\alpha}(\rho), \\ \hat{g}(\rho) &= g(\rho) - \sum_{\alpha} (1 - \mu_{\alpha}^{1/2}) \langle g | \chi^{\alpha} \rangle \chi^{\alpha}(\rho), \end{aligned} \quad (28)$$

which indicate that functions g , \tilde{g} , and \hat{g} have the asymptotic behavior. Definitions (28) show evidence for short-range effects.

In three-body systems, the calculation of μ_α and χ^α must be performed numerically. This issue has been addressed by Varga and Lovas [32] in the GCM formalism for two-cluster systems. I expand the eigenstates $\chi_{\gamma K}^\alpha(\rho)$ [see Eq. (25)] over a GCM basis as

$$\chi_{\gamma K}^\alpha(\rho) = \rho^{5/2} \sum_n C_{\gamma K}^\alpha(R_n) \Gamma_K(\rho, R_n), \quad (29)$$

in analogy with Eq. (15). Then, inserting this expansion in definition (25), I end up with the eigenvalue problem

$$\begin{aligned} \sum_{\gamma' K' R'} [N_{\gamma K, \gamma' K'}^{J\pi}(R_n, R_{n'}) - \mu_\alpha n_{\gamma K, \gamma' K'}^{J\pi}(R_n, R_{n'})] \\ \times C_{\gamma' K'}^\alpha(R_{n'}) = 0, \end{aligned} \quad (30)$$

where the GCM kernel is defined as

$$N_{\gamma K, \gamma' K'}^{J\pi}(R, R') = \langle \Phi_{\gamma K}^{JM\pi}(R) | \Phi_{\gamma' K'}^{JM\pi}(R') \rangle, \quad (31)$$

and is used to determine the generator function in Eq. (11). Matrix n has simple elements

$$\begin{aligned} n_{\gamma K, \gamma' K'}^{J\pi}(R, R') &= \delta_{\gamma \gamma'} \delta_{K K'} \int \Gamma_K(\rho, R) \Gamma_K(\rho, R') d\rho \\ &= (2\pi)^3 \left(\frac{2b^2}{R R'} \right)^2 \exp\left(-\frac{R^2 + R'^2}{4b^2}\right) I_{K+2}\left(\frac{R R'}{2b^2}\right). \end{aligned} \quad (32)$$

The determination of the eigenvalues μ_α and eigenvectors χ^α is therefore straightforward from (30). Notice that, for large values of R_n and $R_{n'}$, the antisymmetrization is negligible and I have, in these conditions,

$$N_{\gamma K, \gamma' K'}^{J\pi}(R, R') \approx n_{\gamma K, \gamma' K'}^{J\pi}(R, R'), \quad (33)$$

which provides a test of the numerical calculation.

The transformed functions \tilde{g} and \hat{g} [see (23)] are expressed as in (15)

$$\begin{aligned} \tilde{g}_{\gamma K}^{J\pi}(\rho) &= \rho^{5/2} \sum_n \tilde{f}_{\gamma K}(R_n) \Gamma_K(\rho, R_n), \\ \hat{g}_{\gamma K}^{J\pi}(\rho) &= \rho^{5/2} \sum_n \hat{f}_{\gamma K}(R_n) \Gamma_K(\rho, R_n), \end{aligned} \quad (34)$$

where the generator functions $\tilde{f}_{\gamma K}(R_n)$ and $\hat{f}_{\gamma K}(R_n)$ are obtained from

$$\begin{aligned} \tilde{f} &= \tilde{M} \cdot f, \\ \hat{f} &= \hat{M} \cdot f. \end{aligned} \quad (35)$$

Matrices \tilde{M} and \hat{M} are defined as

$$\begin{aligned} \tilde{M}_{ij} &= \sum_{\alpha} \mu_{\alpha} C_i^{\alpha} C_j^{\alpha} n_{ij}, \\ \hat{M}_{ij} &= \sum_{\alpha} \mu_{\alpha}^{1/2} C_i^{\alpha} C_j^{\alpha} n_{ij}. \end{aligned} \quad (36)$$

Equations (35) and (36) provide a simple method to determine functions $\tilde{g}^{J\pi}$ and $\hat{g}^{J\pi}$. From these functions, various components can be calculated. For example, the component in the $\alpha = (c, S_1, S_2, S_3, S_{23})$ channel is given by

$$P_{\alpha}^{J\pi} = \sum_{SL\ell_x\ell_y K} \int |\hat{g}_{\gamma K}^{J\pi}(\rho)|^2 d\rho, \quad (37)$$

with

$$\sum_{\alpha} P_{\alpha}^{J\pi} = 1. \quad (38)$$

III. APPLICATIONS

A. Conditions of the calculations

In this section, I apply the formalism to microscopic studies of ${}^6\text{He}$, ${}^{11}\text{Li}$, and ${}^{14}\text{Be}$. The ${}^6\text{He}$ nucleus is a well known halo nucleus and has been investigated in many works (see, for example, Refs. [11,33] and references therein). It will be used as a test of the present formalism. The conditions are those of Ref. [33]: I use the Minnesota nucleon-nucleon interaction [34] with an admixture parameter $u = 1.0045$ and a zero-range spin-orbit force with an amplitude $S_0 = 37 \text{ MeV fm}^5$. In these conditions, the microscopic $\alpha + n + n$ model reproduces the experimental binding energy $E = -0.975 \text{ MeV}$.

From the modified radial functions $\tilde{g}_{\gamma K}^{J\pi}(\rho)$, I can define a two-dimension probability distribution as

$$\mathcal{P}_\alpha^{J\pi}(x, y) = \frac{x^2 y^2}{\rho^5} \int d\Omega_x d\Omega_y \left| \sum_{\ell_x \ell_y LK} \int \tilde{g}_{\gamma K}^{J\pi}(\rho) \varphi_{\gamma K}^{JM\pi}(\Omega_5) \right|^2, \quad (39)$$

with $\rho^2 = x^2 + y^2$, $\alpha = \arctan(y/x)$. The integrals over Ω_x and Ω_y can be performed analytically. I find

$$\mathcal{P}_\alpha^{J\pi}(x, y) = \frac{x^2 y^2}{\rho^5} \sum_{\ell_x \ell_y L} \left| \sum_K \tilde{g}_{\gamma K}^{J\pi}(\rho) F_K^{\ell_x \ell_y}(\alpha) \right|^2, \quad (40)$$

which is normalized as

$$\sum_\alpha \int \mathcal{P}_\alpha^{J\pi}(x, y) dx dy = 1. \quad (41)$$

In practice however, I use the physical coordinates

$$\begin{aligned} r_{nn} &= \sqrt{\mu_{23}} x, \\ r_{c-nn} &= \sqrt{\mu} y, \end{aligned} \quad (42)$$

where r_{nn} is the neutron distance, and r_{c-nn} is the distance between the core and the c.m. of the external neutrons. The modified probability distribution is therefore given by

$$\tilde{\mathcal{P}}_\alpha^{J\pi}(r_{nn}, r_{c-nn}) = \sqrt{\mu_{23}\mu} \mathcal{P}_\alpha^{J\pi} \left(\frac{r_{nn}}{\sqrt{\mu_{23}}}, \frac{r_{c-nn}}{\sqrt{\mu}} \right), \quad (43)$$

where the scaling factor ensures the normalization to unity.

B. Application to ${}^6\text{He}$

In Fig. 1, I present the eigenvalues of the overlap kernel, and some of the corresponding eigenstates. In Fig. 1(a), I limit the number of eigenvalues to 40, for the sake of clarity. Eigenfunction A corresponds to $\mu_\alpha \approx 10^{-8}$ and is plotted in Fig. 1(b) for $\ell_x = \ell_y = K = 0$. When the eigenvalue increases (B,C,D), the range of the eigenfunctions is longer. The property is well known in two-cluster systems, and is extended to three-cluster models. Notice, however, that each eigenfunction contains many (γ, K) values, but a single value is illustrated in the figure. For the eigenfunction D, the main component is in a different channel.

In Fig. 2, I compare the radial functions $\tilde{g}_{\gamma K}^{J\pi}(\rho)$ (solid lines) and $\hat{g}_{\gamma K}^{J\pi}(\rho)$ (dashed lines) for the 0^+ ground state. I illustrate two dominant partial waves: $(\ell_x = \ell_y = 0, K = 2)$ corresponding to $S = 0$, and $(\ell_x = \ell_y = 1, K = 2)$ corresponding to $S = 1$. The dotted lines are obtained in a nonmicroscopic $\alpha + n + n$ model [35]. They are close to the microscopic $\hat{g}_{\gamma K}^{J\pi}$ functions, which is not surprising since both are normalized to unity. Functions $\tilde{g}_{\gamma K}^{J\pi}$, however, are different at short distances, due to antisymmetrization effects. The long-range parts of $\tilde{g}_{\gamma K}^{J\pi}$ and of $\hat{g}_{\gamma K}^{J\pi}$ are identical, as expected.

Figure 3 presents the probability distributions (43) for $S = 0$ and $S = 1$. The $S = 0$ probability is similar to previous nonmicroscopic [3,35] and microscopic [36] results with two maxima, corresponding to the so-called ‘‘dineutron’’ ($r_{nn} \approx 2.5$ fm) and ‘‘cigar’’ ($r_{nn} \approx 4.0$ fm) configurations. The $S = 1$ amplitude is smaller, as the wave function contains 86% of

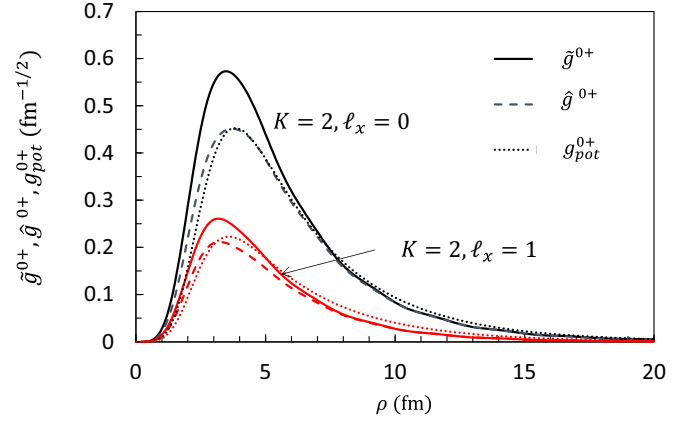


FIG. 2. Hyperradial functions \tilde{g} and \hat{g} for the ${}^6\text{He}$ ground state, as well as non-microscopic approximation (g_{pot} ; see text). The dominant partial waves $S_{23} = 0, K = 2, \ell_x = \ell_y = 0$ (black) and $S_{23} = 1, K = 2, \ell_x = \ell_y = 1$ (red) are shown.

$S = 0$ and 14% of $S = 1$, which is consistent with nonmicroscopic approaches.

C. Application to ${}^{14}\text{Be}$

The conditions of the calculations are those of Ref. [14]. I use R_n values from 1.5 to 15 fm by steps of 1.5 fm, with $K_{\text{max}} = 16$. The nucleon-nucleon interaction is the Volkov V2 force with $M = 0.6119$ and includes a spin-orbit force with an amplitude $S_0 = 40$ MeV fm⁵. With these conditions, the ground-state binding energy is $S_{2n} = 1.12$ MeV, in agreement

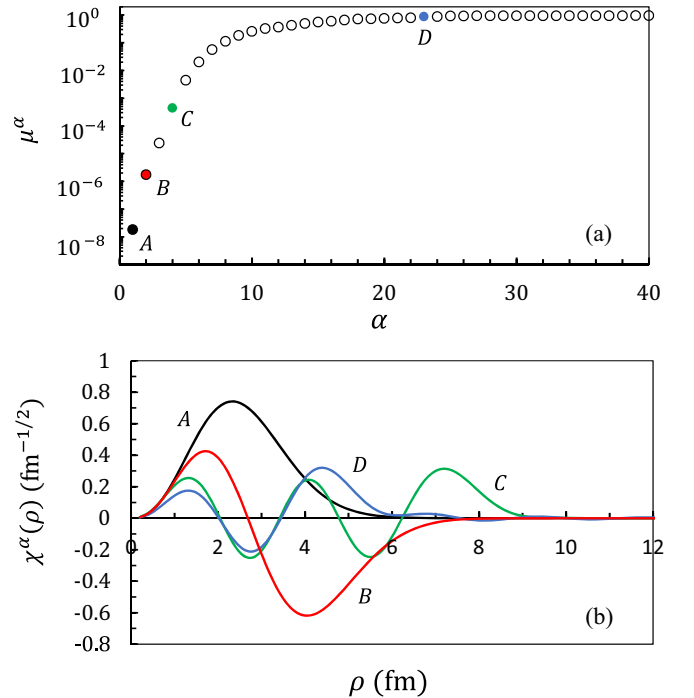


FIG. 1. (a) Eigenvalues μ_α of ${}^6\text{He}$ ($J = 0^+$). Notice that only 40 eigenvalues are shown. (b) Corresponding functions $\chi_{\gamma K}^\alpha(\rho)$ [see Eq. (24)] for $\ell_x = \ell_y = K = 0$.

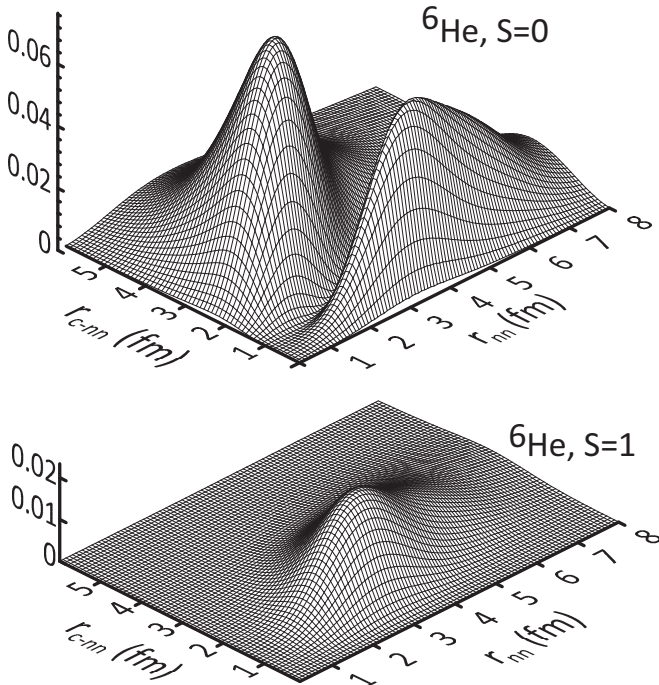


FIG. 3. Probability distribution $\hat{P}_\alpha^{J\pi}(r_m, r_{c-m})$ of the ${}^6\text{He}$ ground state for $S = 0$ and $S = 1$.

with experiment. The calculation involving the p shell for ${}^{12}\text{Be}$ provides 15 Slater determinants corresponding to two 0^+ states, one 1^+ state, and two 2^+ states. For the sake of completeness, I compare the multichannel calculation to the single-channel approximation, which involves the ${}^{12}\text{Be}(0_1^+) + n + n$ configuration only. In that case, the Majorana parameter is modified to $M = 0.59$ in order to keep the same binding energy.

In Table I, I present the probabilities (37) associated with the core states. I separate the contributions from $S_{23} = 0$ and from $S_{23} = 1$. In all cases, the $S_{23} = 1$ component is small. In the multichannel calculation, the ground-state configuration is dominant, with 12% of the ${}^{12}\text{Be}(2^+)$ excited state. Other states (0_2^+ , 1^+ , 2_2^+) correspond to pseudostates, and improve the description of ${}^{14}\text{Be}$. However, they do not have experimental counterparts.

Figure 4 presents the K components of the ${}^{14}\text{Be}$ ground state, with a separation between the core states. As expected from Table I, the ${}^{12}\text{Be}$ ground state is dominant. However, the 2_1^+ component is not negligible for $K = 2$ and $K = 4$.

In Fig. 5, I display some radial functions $\tilde{g}_{\gamma K}$ (solid lines) and $\hat{g}_{\gamma K}$ (dashed lines). In each case, I show the single and multichannel results and illustrate $K = 0$ and $K = 4$, which

TABLE I. ${}^{14}\text{Be}$ occupancy probabilities (37) for different core states S_1 and neutron-neutron coupling spins S_{23} .

S_1	$S_{23} = 0$	$S_{23} = 1$
0^+	0.843	0.017
2^+	0.122	0.012

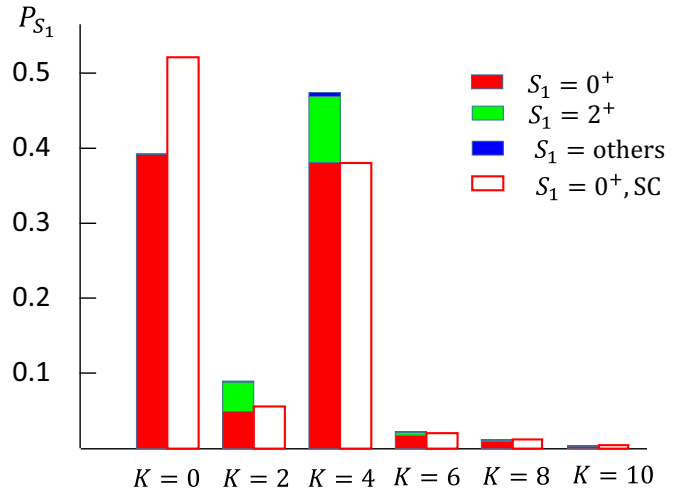


FIG. 4. K components in the ${}^{14}\text{Be}$ ground state for the multi-channel model (left columns) and for the single-channel model (right columns). The probabilities associated with the ${}^{12}\text{Be}$ core states are shown in different colors. The single-channel calculation is labeled as ‘‘SC.’’

are the dominant hypermomenta. In agreement with Table I, the single and multichannel functions are similar.

Figure 6 represents the density distributions (43) for $S_1 = 0^+$ and $S_1 = 2^+$. In both cases, I select $S_{23} = 0$ which is the main component. Both probabilities present three peaks. This figure shows that reproducing accurately the wave function at large distances is fundamental. Large neutron-neutron coordinates (up to $r_m \approx 10$ fm) play a role.

D. Application to ${}^{11}\text{Li}$

As for ${}^{14}\text{Be}$, I use the conditions of calculations of Ref. [14]. In this case, the ${}^9\text{Li}$ core involves 90 Slater determinants in the p shell, and the calculations are much longer. After diagonalization, I keep $S_1 = 3/2^-$ and $S_1 = 1/2^-$ states,

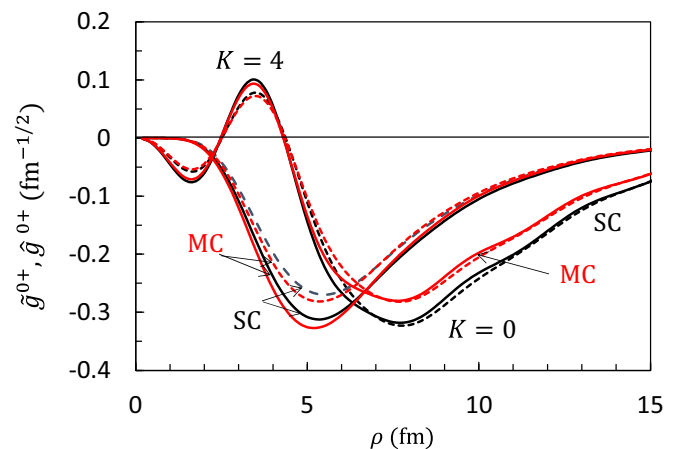


FIG. 5. Multichannel (MC, red color) and single-channel (SC, black color) functions $\tilde{g}_{\gamma K}(\rho)$ (solid lines) and $\hat{g}_{\gamma K}(\rho)$ (dashed lines) in the ${}^{14}\text{Be}$ ground state. The dominant partial waves are $K = \ell_x = \ell_y = 0$ and $K = 4$, $\ell_x = \ell_y = 2$.

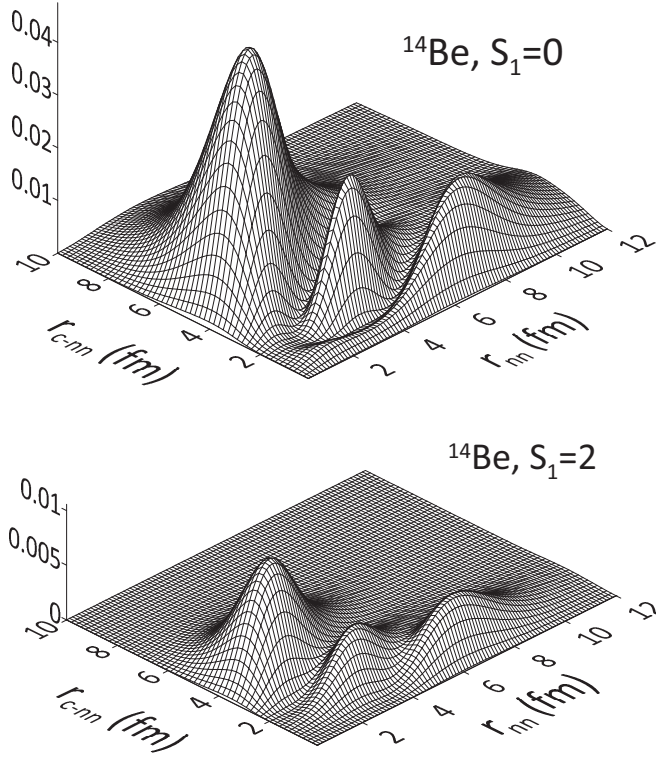


FIG. 6. Probability distribution $\hat{P}_\alpha^{J\pi}(r_{nn}, r_{c-nn})$ of the ^{14}Be ground state. The upper and lower figures correspond to the $S_1 = 0^+$ and $S_1 = 2^+$ core states, respectively. In both cases, the external neutrons are coupled to $S_{23} = 0$.

which correspond to the ground and first excited states of ^9Li . Notice that other $3/2^-$ and $1/2^-$ eigenvalues arise from the diagonalization. They do not have experimental counterparts, but contribute to the ^{11}Li wave function.

In Table II, I discuss the probabilities (37) for the different core states and for the neutron-neutron spin $S_{23} = 0$ and 1. In this case, the $^9\text{Li}(\text{gs}) + n + n$ component is only 50% of the total wave function, which means that core excitations are quite important. Without core excitations and with the same nucleon-nucleon interaction, the ^{11}Li ground state is unbound (+0.61 MeV). As in ^{14}Be the spin coupling $S_{23} = 0$ is dominant.

Figure 7 displays the K components of the ^{11}Li ground state for the multichannel and single channel calculations. In the latter case, the Majorana parameter has been slightly modified to reproduce the two-neutron separation energy ($M = 0.741$). I find that $K = 2$ is dominant with a small contribution of $K = 0$ and of $K = 4$. Other K values are negligible.

TABLE II. ^{11}Li occupancy probabilities (37) for different core states S_1 and neutron-neutron coupling spins S_{23} .

S_1	$S_{23} = 0$	$S_{23} = 1$
$3/2^-$	0.498	0.073
$1/2^-$	0.018	0.019
$3/2^-$ (others)	0.160	0.155
$1/2^-$ (others)	0.020	0.058

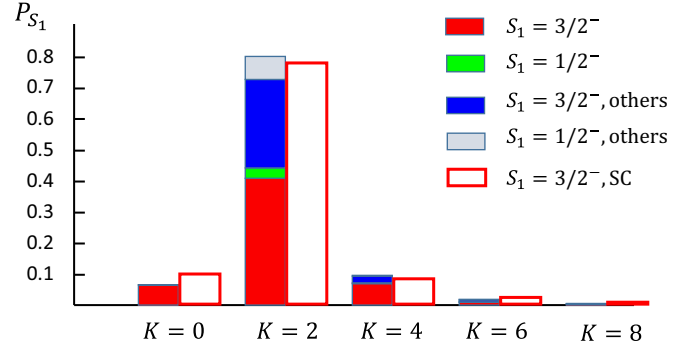


FIG. 7. See caption to Fig. 4 for the ^{11}Li ground state.

In Fig. 8, I present radial functions $\tilde{g}_{\gamma K}(\rho)$ (solid lines) and $\hat{g}_{\gamma K}(\rho)$ (dashed lines) for the $^9\text{Li}(\text{gs}) + n + n$ configuration. I illustrate the multichannel (MC) and single-channel (SC) calculations. For the dominant component $K = 2$ the difference is rather large, as expected from Table II.

Figure 9 displays the density distribution (43) associated with the ^9Li ground state (upper panel) and with the first $3/2^-$ excited state (lower panel), which represent the main contributions to the wave functions (see Table II). In both cases, I select $S_{23} = 0$. The maximum of the density distribution is located at large distances ($r_{nn} = 2.3$ fm, $r_{c-nn} = 4.0$ fm), which is consistent with the halo interpretation of ^{11}Li .

IV. CONCLUSION

In this paper, I have developed a technique to determine spectroscopic amplitudes of three-body systems in the microscopic three-cluster RGM/GCM method. This approach is based on an effective nucleon-nucleon interaction and on a cluster structure of the nucleus. The core nucleus is described by a combination of shell-model states, and includes not only the ground state, but also excited states. The model requires

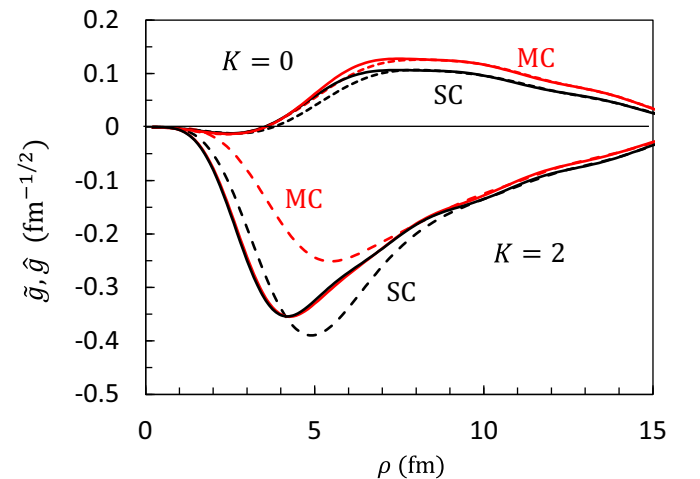


FIG. 8. Multichannel (MC, red color) and single-channel (SC, black color) functions $\tilde{g}_{\gamma K}(\rho)$ (solid lines) and $\hat{g}_{\gamma K}(\rho)$ (dashed lines) in the ^{11}Li ground state.

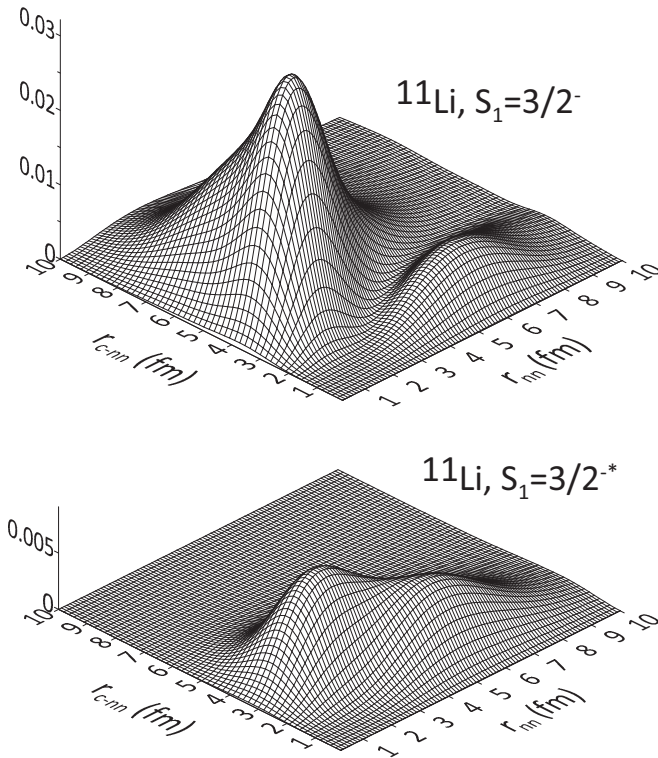


FIG. 9. Probability distribution $\tilde{\mathcal{P}}_{\alpha}^{J\pi}(r_m, r_{c-m})$ of the ^{11}Li ground state. The upper and lower figures correspond to the $S_1 = 3/2^-$ ^9Li ground state and $S_1 = 3/2^-$ first excited state states, respectively. In both cases, the external neutrons are coupled to $S_{23} = 0$.

long computer times and large memories, but can be applied with modern computing facilities.

The main goal of this work is to provide approximations of the relative wave functions, where the antisymmetrization is simulated by an appropriate transformation of the wave functions. This technique represents an extension of previous works developed for two-cluster systems [5,16,17]. It is based on the eigenvalues and eigenfunctions of the overlap kernel. These quantities can be calculated numerically. The transformed wave functions provide overlap integrals and probability distributions, which help to analyze the structure of the nucleus, and in particular the role of the core excitations. I have shown that core excitations are quite important in ^{11}Li (about 50%), but play a smaller role in ^{14}Be (12%).

In scattering theory, the use of overlap integrals and spectroscopic factors is widespread (see, for example, Ref. [20] and references therein). At the DWBA approximations, they are essentially used to determine one-nucleon transfer cross sections. The present work paves the way to more ambitious calculations involving two-nucleon transfer reactions. A typical example is the $^{11}\text{Li}(p, t)^9\text{Li}$ cross section, which has been measured [37], but its theoretical description using a nonmicroscopic $^9\text{Li}+n+n$ model of ^{11}Li is not fully satisfactory [38]. Works in this direction are in progress.

ACKNOWLEDGMENTS

This work was supported by the Fonds de la Recherche Scientifique–FNRS under Grants No. 4.45.10.08 and No. J.0065.22. It benefited from computational resources made available on the Tier-1 supercomputer of the Fédération Wallonie-Bruxelles, infrastructure funded by the Walloon Region under Grant Agreement No. 1117545.

- [1] I. Tanihata, H. Savajols, and R. Kanungo, *Prog. Part. Nucl. Phys.* **68**, 215 (2013).
- [2] L. F. Canto, P. R. S. Gomes, R. Donangelo, J. Lubian, and M. S. Hussein, *Phys. Rep.* **596**, 1 (2015).
- [3] M. V. Zhukov, B. V. Danilin, D. V. Fedorov, J. M. Bang, I. J. Thompson, and J. S. Vaagen, *Phys. Rep.* **231**, 151 (1993).
- [4] K. Wildermuth and Y. C. Tang, *A Unified Theory of the Nucleus*, edited by K. Wildermuth and P. Kramer (Vieweg, Braunschweig, 1977).
- [5] H. Horiuchi, *Prog. Theor. Phys. Suppl.* **62**, 90 (1977).
- [6] P. Descouvemont and M. Dufour, *Microscopic cluster models, Clusters in Nuclei* (Springer, Berlin, Heidelberg, 2012), pp. 1–66.
- [7] H. Horiuchi, K. Ikeda, and K. Katō, *Prog. Theor. Phys. Suppl.* **192**, 1 (2012).
- [8] P. Navrátil, S. Quaglioni, G. Hupin, C. Romero-Redondo, and A. Calci, *Phys. Scr.* **91**, 053002 (2016).
- [9] Y. Fujiwara, H. Horiuchi, K. Ikeda, M. Kamimura, K. Katō, Y. Suzuki, and E. Uegaki, *Prog. Theor. Phys. Suppl.* **68**, 29 (1980).
- [10] Y. Fujiwara and Y. C. Tang, *Phys. Rev. C* **31**, 342 (1985).
- [11] K. Arai, Y. Suzuki, and R. G. Lovas, *Phys. Rev. C* **59**, 1432 (1999).
- [12] K. Varga, Y. Suzuki, and R. G. Lovas, *Phys. Rev. C* **66**, 041302(R) (2002).
- [13] S. Korennov and P. Descouvemont, *Nucl. Phys. A* **740**, 249 (2004).
- [14] P. Descouvemont, *Phys. Rev. C* **99**, 064308 (2019).
- [15] C. D. Lin, *Phys. Rep.* **257**, 1 (1995).
- [16] S. Saito, *Prog. Theor. Phys.* **41**, 705 (1969).
- [17] H. Friedrich, *Phys. Rep.* **74**, 209 (1981).
- [18] D. Baye and P. Descouvemont, *Ann. Phys. (NY)* **165**, 115 (1985).
- [19] D. Baye and M. Kruglanski, *Phys. Rev. C* **45**, 1321 (1992).
- [20] N. K. Timofeyuk, *J. Phys. G* **41**, 094008 (2014).
- [21] P. Descouvemont, *Eur. Phys. J. A* **58**, 193 (2022).
- [22] P. Descouvemont, *Nucl. Phys. A* **596**, 285 (1996).
- [23] K. Varga, Y. Suzuki, and Y. Ohbayasi, *Phys. Rev. C* **50**, 189 (1994).
- [24] K. Arai, Y. Ogawa, Y. Suzuki, and K. Varga, *Prog. Theor. Phys. Suppl.* **142**, 97 (2001).
- [25] J. Raynal and J. Revai, *Nuovo Cim. A* **68**, 612 (1970).
- [26] A. Dammann and P. Descouvemont, *Phys. Rev. C* **80**, 044310 (2009).
- [27] V. Vasilevsky, A. V. Nesterov, F. Arickx, and J. Broeckhove, *Phys. Rev. C* **63**, 034607 (2001).

- [28] P. Descouvemont, E. M. Tursunov, and D. Baye, *Nucl. Phys. A* **765**, 370 (2006).
- [29] D. Baye and N. K. Timofeyuk, *Phys. Lett. B* **293**, 13 (1992).
- [30] I. Brida, S. C. Pieper, and R. B. Wiringa, *Phys. Rev. C* **84**, 024319 (2011).
- [31] Y. Suzuki, R. G. Lovas, K. Yabana, and K. Varga, *Structure and Reactions of Light Exotic Nuclei* (Taylor & Francis, London, 2003).
- [32] K. Varga and R. G. Lovas, *Phys. Rev. C* **37**, 2906 (1988).
- [33] M. Theeten, D. Baye, and P. Descouvemont, *Phys. Rev. C* **74**, 044304 (2006).
- [34] D. R. Thompson, M. LeMere, and Y. C. Tang, *Nucl. Phys. A* **286**, 53 (1977).
- [35] P. Descouvemont, C. Daniel, and D. Baye, *Phys. Rev. C* **67**, 044309 (2003).
- [36] S. Quaglioni, C. Romero-Redondo, and P. Navrátil, *Phys. Rev. C* **88**, 034320 (2013).
- [37] I. Tanihata, M. Alcorta, D. Bandyopadhyay, R. Bieri, L. Buchmann, B. Davids, N. Galinski, D. Howell, W. Mills, S. Mythili, R. Openshaw, E. Padilla-Rodal, G. Ruprecht, G. Shiffer, A. C. Shotton, M. Trinczek, P. Walden, H. Savajols, T. Roger, M. Caamano, W. Mittig, P. Roussel-Chomaz, R. Kanungo, A. Gallant, M. Notani, G. Savard, and I. J. Thompson, *Phys. Rev. Lett.* **100**, 192502 (2008).
- [38] P. Descouvemont, *Phys. Rev. C* **104**, 024613 (2021).